

FINAL REPORT

FFG Projektnummer	878151	FörderungsnehmerIn	ÖBV
Bericht Nr.	1	Berichtszeitraum	01.10.2020 – 30.09.2021
Bericht erstellt von	Pauser, Robisson		

Richtwert für den Umfang: 10-20 Seiten

1. Ziele und Ergebnisse

- Wurden die dem Förderungsvertrag zugrunde liegenden Ziele erreicht? Sind diese Ziele noch aktuell bzw. realistisch?
Achtung: Änderungen von Zielen erfordern eine Genehmigung durch die FFG.
- Vergleichen Sie die Ziele mit den erreichten Ergebnissen.
- Beschreiben Sie „Highlights“ und aufgetretene Probleme bei der Zielerreichung.

This third year's achievements include:

- Identification of two setups (Le Chatelier ring and oedometer) to evaluate internal sulfate attacks. Preliminary results with both methods seem to correlate, at least qualitatively.
- Elucidation of the detrimental effect of temperature on concrete-epoxy-concrete elements. Experiments were performed on single components and the dominating factor was identified as the lack of common window time for cement and epoxy settings.
- Proposal of a new construction method to produce lightweight thermally insulating structural concretes with an infiltration process. Fabrication of a laboratory setup as a proof-of-concept.
- Identification of non-homogeneous shear during rheological tests using the parallel plate geometry that can explain the detrimental effects of pre-shear on last year results. This heterogenous flow of cement-based slurries may be a signature of their behavior and will be investigated further.
- Quantitative measurement of silica fume de-agglomeration during UHPC dry mixing
- Identification of reliable protocols in rheology to assess the yield stress of cementitious pastes.
- Demonstration of different deformation behaviors (and particle interactions) in Portland cement and alkali-activated pastes using small amplitude oscillatory rheology
- Identification of an calcium-based additive to make PCE superplasticizers effective in alkali-activated materials.

Specific work packages are described in section 2.2. The work packages were incorporated into the 4 sub-projects, with project abstracts in the next pages.

Team (co-authors of reports) is composed of Dana Daneshvar, Karl Deix, Subhransu Dhar, Johannes Kimbauer, Teresa Liberto, Agathe Robisson.

Projekt 1: Interner Sulfatangriff: Ein Problem bei rezyklierten Gesteinskörnungen (RGK)? (AP5, AP7)

Teresa Liberto, Johannes Kirnbauer, Agathe Robisson

Zusammenfassung

Die Verwendung von rezyklierten Gesteinskörnungen (RGK) in neuen Bauwerken begann nach dem Zweiten Weltkrieg und wird seither mit Unterbrechungen eingesetzt. Das aktuelle Interesse an RGK steht im Zusammenhang mit der ökologischen Notlage, in der sich unser Planet befindet, und der Notwendigkeit, die mit der CO₂-Produktion von neuem Zementklinker verbundenen Emissionen zu verringern.

Ein Phänomen, das die Dauerhaftigkeit von Beton stark beeinträchtigt und zu einer Verschlechterung und schweren strukturellen Schäden führen kann, ist der Sulfatangriff (SA). Externer Sulfatangriff ist mit (externen) Umweltfaktoren verbunden, während interner Sulfatangriff (ISA) von der Betonzusammensetzung (d. h. dem Sulfatgehalt) abhängt. In beiden Fällen können Sulfate (aus einer externen oder internen Quelle) mit Restaluminiumverbindungen reagieren und verzögert Ettringit bilden, das eine Volumenausdehnung und folglich Rissbildung verursacht. ISA kann auftreten, wenn RGK, das bei neuen Mischungen verwendet wird, mit Gips verunreinigt ist, was zu einer frühzeitigen Verschlechterung führt. Der Mangel an Wissen über ISA auf Beton und ihre Gefährlichkeit bei der Verwendung von RGK war der Grund für diese Studie. Zur Quantifizierung der ISA-bedingten Ausdehnung von Mörtel und Recyclingbeton werden verschiedene Methoden angewandt, wie z. B. die Variation der Prismenlänge, Le-Chatelier-Ausdehnungsringe und eine in eine Druckvorrichtung integrierte Ödometerzelle. Insbesondere untersuchen wir den Einfluss von Schlüsselvariablen wie Wasser-Zement-Verhältnis W/C, Zementtyp, Zementhydratationszustand, Aushärtungs- und Umgebungsbedingungen, Gipsgehalt und Feinheit auf die ISA.



Projekt 2: Nachhaltiger Beton und Messung der Fließspannung

Projekt 2a - Messungen der Fließspannung in Zementschlämme (AP3)

Subhransu Dhar, Teresa Liberto, Agathe Robisson

Projekt 2b - Alkalisch-aktivierte Bindemittel: eine Fallstudie zu Fließspannung und Elastizitätsmodul (AP5)

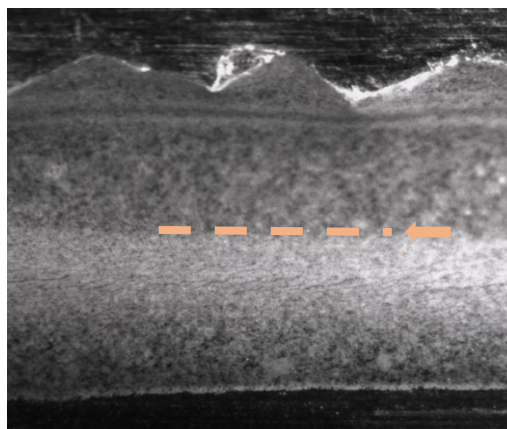
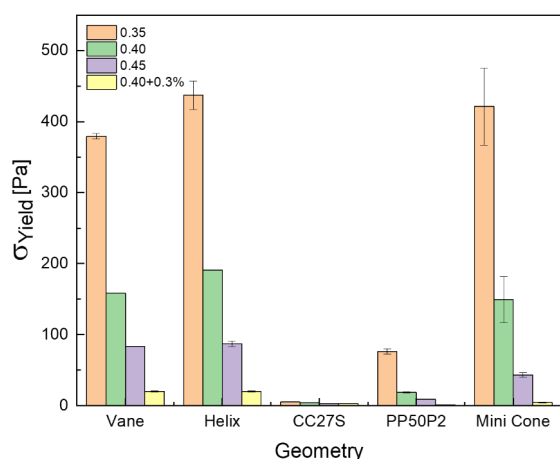
Teresa Liberto, Maurizio Bellotto, Agathe Robisson

Zusammenfassung

Die Fließspannung von dichten Suspensionen entsteht durch die Wechselwirkungen zwischen den Partikeln und speziell bei Zement durch die Wechselwirkungen zwischen den Zementkörnern durch die stark ionische Porenlösung und durch die Nanohydrate von C-S-H, die sich unmittelbar nach der Wasserzugabe bilden. In den folgenden Arbeitspaketen (WP3 und WP5) befassen wir uns mit zwei entscheidenden Aspekten, die für die Charakterisierung und das Verständnis dieser Wechselwirkungen von grundlegender Bedeutung sind: Wir untersuchen die Fließspannung mit Hilfe der Rotationsrheologie, um schließlich ein Protokoll für eine reproduzierbare und genaue Messung vorzuschlagen, und wir entwickeln eine Methode zur Untersuchung der Partikelwechselwirkungen in verschiedenen zementhaltigen Materialien in der ersten Stunde nach dem Mischen unter Verwendung der Oszillationsrheologie.

Unsere Ergebnisse aus Projekt 2a zeigen, dass die Messung der Fließspannung mit einem Rheometer sehr sorgfältige Experimente erfordert. In der Tat haben wir unter Verwendung der lokalen Bildgebung auf einer parallelen Plattengeometrie die Bildung von Scherbändern beobachtet. Andererseits führen die Geometrien Helix und Vane zu einer Messung der Fließspannung, die der Messung der Kegelausbreitung ähnelt.

In Bericht 2b zeigen wir eine Fallstudie, in der das Verhalten eines normalen Portlandzements mit einem alkalisch aktivierten Bindemittel (AAB) verglichen wird. Im Vergleich zu Schaumstoffen aus Portlandzement können AAB-Schaumstoffe in der Tat erhebliche Vorteile bieten (Dhasindrakrishna et al., 2019), aber die Art der Partikelinteraktionen wurde noch weniger untersucht. Unsere Ergebnisse geben auch Aufschluss über die Auswirkungen von Zusatzstoffen wie Fließmittel auf AABs.



Projekt 3: Mörtelinjektion für halbfeste Beschichtungen, Wärmedämmstoffe und Gebäudesanierung (AP7)

Teresa Liberto, Johannes Kirnbauer, Agathe Robisson

Zusammenfassung

Wir schlagen hier eine neuartige Methode zur Herstellung von leichtem, wärmeisolierendem Konstruktionsbeton durch ein Infiltrationsverfahren vor, bei dem die leichten Gesteinskörnungen die Struktur oder Schalung vorfüllen und der Zementschlamm von unten gepumpt wird.

Wir untersuchten Blähtonperlen als leicht Gesteinskörnung (LGK). Wir haben gezeigt, dass sie in den ersten Sekunden der Wassereinwirkung 10-12 Gew.-% Wasser aufnehmen.

Wir bauten einen Infiltrationsaufbau, bei dem der Schlamm von unten infiltriert wurde. In der Tat haben wir gemessen, dass, wenn ein Schlamm durch die nicht vorgemästen Aggregate gepumpt wurde, eine Filtration stattfand, die zu einer Eindickung des Schlamms führte, der schließlich den Durchfluss verstopfte. Wir haben auch gezeigt, dass die Vorbefeuchtung zu einer heterogenen Zusammensetzung führen kann, was die Festigkeit des ausgehärteten Betons verringern könnte.

Wichtig ist, dass wir einen vielversprechenden Zusatzstoff identifiziert haben, der es einer Zementschlämme ermöglichte, eine 85 cm hohe Packung nicht vorgemäster LGK problemlos zu infiltrieren, während dies bei allen anderen Schlämmen (auch wenn sie Fließmittel enthielten) nicht gelang.

Wir haben uns nicht darauf konzentriert, die Packung der leichten Gesteinskörnungen zu maximieren, aber diese vorläufigen Ergebnisse zeigen, dass diese neuartige Methode einen höheren Gehalt an porösen Gesteinskörnungen ermöglichen kann, als die üblichen Mischmethoden, bei denen der Beton fließen muss.



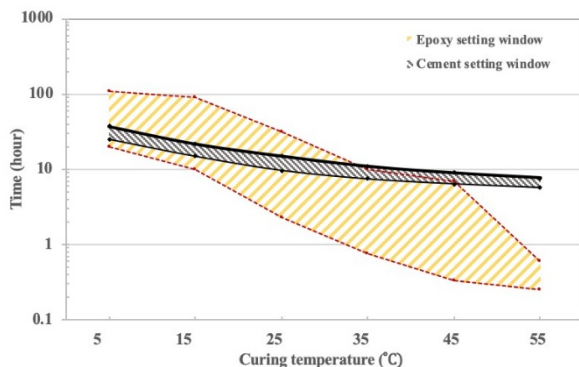
Projekt 4: Charakterisierung der Grenzfläche von Beton zu Beton: Experimentelle Bewertung des Temperatureinflusses auf die Haftfestigkeit der Grenzfläche (AP6)

D. Daneshvar, K. Deix, A. Robisson

Zusammenfassung

Die Gieß- und Aushärtungstemperatur hat einen erheblichen Einfluss auf die Verbundfestigkeit zwischen Beton und Epoxidharz. Auf der Suche nach den Hauptursachen wurden die einzelnen in den Beton-Beton-Verbundwerkstoffen verwendeten Materialien, d. h. Epoxidharz und Zementleim anhand von Messungen der Viskosität, der Shore-D-Härte und der Abbindezeit charakterisiert. Um ein breites Spektrum an klimatischen Bedingungen abzudecken, wurden sechs verschiedene Temperaturwerte von 5 bis 55 °C berücksichtigt. Die Ergebnisse zeigen, dass die deutlich kürzere Abbindezeit von Epoxidharz im Vergleich zu Zement bei hohen Temperaturen die schlechteren mechanischen Eigenschaften von Epoxidharz sowie die Verringerung der Epoxidharzdicke aufgrund von Materialverlust in Poren und Mikrorissen diesen Rückgang erklären können.

Diese Ergebnisse liefern uns wichtige Informationen über vielversprechende Wege zur Optimierung der Epoxidharz-Beton-Verbindungen. Die beiden wichtigsten Möglichkeiten sind entweder die Kontrolle der Temperatur während des Gießens und Aushärtens oder eine bessere Abstimmung der Abbindezeiten von Epoxid und Zement. Insbesondere wird empfohlen, dass die Untergrundtemperatur zum Zeitpunkt des Gießens des Belags 35 °C nicht überschreitet. Zusätzlich zur Temperaturkontrolle könnten die erheblichen Unterschiede bei der Abbindezeit unter heißen Bedingungen entweder durch eine Beschleunigung der Zementhydratation, oder durch eine Verzögerung der Epoxidaushärtung gemildert werden.



2. Arbeitspakete und Meilensteine

2.1 Übersichtstabellen

Erläuterung:

Die Tabellen sind analog zum Förderungsansuchen aufgebaut.
 Basistermin: Termin laut Förderungsansuchen bzw. laut Vertrag gültigem Projektplan
 Aktuelle Planung: Termin laut zum Zeitpunkt der Berichtslegung gültiger Planung

Tabelle 1: Arbeitspakete

AP No.	work package designation	Degree of completion	base date		Current		Achieved results / deviations
			start	end	start	end	
1	Project management	40%	10.18	09.23	10.18	09.23	Mid-year 3 meeting held 17.05.2021 on-line. End of year 3 meeting planned 28.09.2021.
2	State of the art	80%	10.18	09.19	10.18	09.23	Examination of EU legislation for recyclability in construction, foam cement, durability of recycled aggregate concrete continues with each step of the research projects.
3	Entwicklung rheo-logischer Prüfungen und Verfahren Development of rheological tests and procedures	75%	10.18	09.21	10.18	09.23	Four geometries of the rheometer were used to measure yield stress, and results were benchmarked against the yield stress calculated from spread. Visualization of slurry flow in a parallel plate geometry could explain unsatisfactory results obtained with this geometry. Given the heterogeneities of cement flow observed with this geometry, LAOS was not explored further.
4	Untersuchung des Einflusses des Mischvorgangs Investigation of the influence of the mixing process	100%	10.18	09.21	10.18	09.21	A proper protocol was identified on the Mastersizer, highlighting the importance of the obscuration parameter. Dry mixes were analyzed with the proper obscuration value and results are trusted as quantitative. The analysis clearly shows that increasing dry mixing time increases the volume fraction of deagglomerated silica fume, and in turn the packing density. They also show the superior character of the EIRICH mixer for a quicker de-agglomeration. Specifically, a 15 min high intensity dry mixing leads to de-agglomerate about 70 % of the silica fume, a time deemed sufficient to prepare dry

							mixes that can then be wet-mixed with conventional mixers.
5	Einfluss der Zementpartikelgrößen-verteilung und beschaffenheit (Vorhandensein von nachhaltigen Bindemitteln) auf die Betonrheologie, die Schäumbarkeit, und das Erstarrungsverhalten Influence of cement particle size distribution and nature (presence of sustainable binders) on concrete rheology, foamability, and setting properties	75%	10.18	09.20	10.18	09.23	Yield stress of Portland cement slurries at different w/c ratios and amounts of superplasticizers, as well as alkali-activated binders with different amounts of superplasticizers were measured. In some of these slurries, the evolution of elastic modulus with time at rest (i.e. structuration) is measured. Using oscillatory rheological as a quantitative method, we demonstrated that upon addition of calcium ions, alkali-activated based slurries could respond to a superplasticizer. The reactivity of samples made of a blend of gypsum powder and hydrated concrete powder mixed with water was assessed using oscillatory rheology. Results do not follow a rule of mixture, indicating further chemical reaction, and require further work to be explained. Preliminary calorimetry and XRD results are briefly presented.
6	Schnittstellen zwischen altem Material und neuem Beton Interfaces between old material and new concrete	80%	10.18	09.23	10.18	09.22	Hardening time of epoxy and setting time of concrete were individually assessed at 6 different temperatures and compared. The lack of overlapping time window for hardenings of cement and epoxy at high temperature can explain the poor interfacial strength measured. Additionally, the average epoxy interface thickness between old and new concrete was measured and decrease with casting temperature, further explaining the strength decrease. Analytical model from year 1 were not revisited at this point.
7	Einrichtung zur Messung der Infiltration Device for the measurement of infiltration	50%	10.19	10.22	07.20	10.23	A setup for infiltration was built where the slurry penetrated from bottom up under pressure. Results show that smaller aggregates are harder to infiltrate than larger ones, and that pre-wetting the porous aggregates is very favorable to slurry penetration. Only one slurry could infiltrate a pack of lightweight aggregates that were not pre-

							wetted: it contains an additive that was designed for the oilfield and allowed the slurry to progress within the porous aggregates without de-watering. Finally, the bottom infiltration setup showed it was possible to produce homogeneous lightweight concretes with minimal defects (no water trapped), making this method a potential manufacturing technique.
8	Equipment for the production of cement foams	100% / stopped	10.19	10.20	10.19	10.20	Stopped
9	Device for characterizing volume changes or limiting pressure of RA concretes	40%	10.19	10.23	10.19	10.23	Gypsum was added to various cement types containing increasing amount of aluminate phases. Expansion upon water exposure was measured with Le Chatelier rings. Confining pressure was measured with an oedometer. Results seem correlated, at least qualitatively. They also show that both expansion and swelling pressure increase with increasing aluminate content in the cement.
10	High thermal insulation in a double walled tower	0%	10.22	10.23	10.22	10.23	This work package starts in the last year of research

2.2 Description of the work carried out during the reporting period

AP 3: Development of rheological tests and procedures

In the previous report, the effect of a pre-shearing step on the growth of elastic modulus of cement pastes was studied. The pre-shear was applied within the serrated parallel plates of a rheometer by applying 100 % strain amplitude cycles, and was meant to erase previous shear and rest history of the paste. It was observed that with longer duration of pre-shear (~300 s), the growth of elastic modulus was low and never attained expected values, even with ample amounts of time given for the paste structuration, contradicting the typical behavior of cement pastes (Yuan et al., 2017). Hence, we decided to look at the local shear behavior of the paste using optical techniques. Via imaging, we observed that within seconds of the application of shear, only a small part of the sample near the upper moving plate seemed to be sheared, indicating that a lubrication layer may have formed within the paste, near the moving top plate. In other words, all shear seems to happen within this top layer while the rest of the sample looked static. This observation is critical because the data treatment based on the assumption that the whole sample is sheared will be erroneous.

Based on these results, we decided to extend our investigation to the dynamic yield stress behavior of cement pastes using four different geometries, namely, vane, helical, sand blasted small gap concentric cylinders (Couette) and serrated parallel plates. These

geometries create different shear rate distributions in the sample, and we hypothesize that the formation of shear bands may not occur in some of these geometries, making them more desirable for reliable yield stress measurement.

Finally, to relate the yield stress values obtained from different geometries, we measured a yield stress using mini-cone slump test, an easy measurement used on construction sites. The results obtained show that the vane and helical geometries exhibit similar values of yield stress as that of mini-cone slump tests, whereas the values obtained with the concentric cylinders and parallel plates geometries are suspiciously low.

Materials and Methods

Slurries were prepared using CEM I (Contragress cement powder 42.5 R-SR 0 WT 27 C3A-free, Lafarge-Holcim) in distilled water (room temperature) with w/c ratio of 0.35, 0.40 and 0.45. Additionally, a low yield stress specimen is obtained by adding 0.3 % of PCE (polycarboxylate ether, MasterGlenium® ACE 430) in the w/c=0.4 cement paste. To measure yield stress with the rheometer, a logarithmically decreasing shear stress ramp was imposed while the shear rate was recorded. The resulting shear rate (red line) vs shear stress (black line) graph was used to determine the yield stress of the cement paste (Fig. 3.1) using the minimum of the double derivative of shear rate with time and recording the stress at this time.

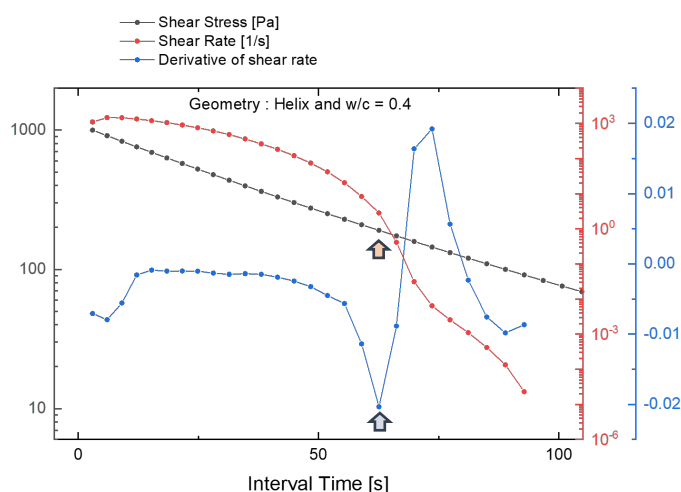


Fig 3.1: Imposed logarithmically decreasing shear stress (black), measured shear rate (red) and double derivative of log of shear rate (blue) as a function of time for helical geometry with w/c = 0.40. Yield stress is found around 200 Pa (arrow).

Yield stress was also measured with a mini-cone spread test from which yield stress is calculated (Roussel et al. 2005, Tan et al. 2017).

In order to observe the behavior of the cement paste within the plates during rheological measurements, a high-speed camera with a magnifying lens is used.

Results

Yield stresses obtained by rheological measurements with different geometries and by mini-cone slump tests are shown in the form of a histogram Fig. 3.2.

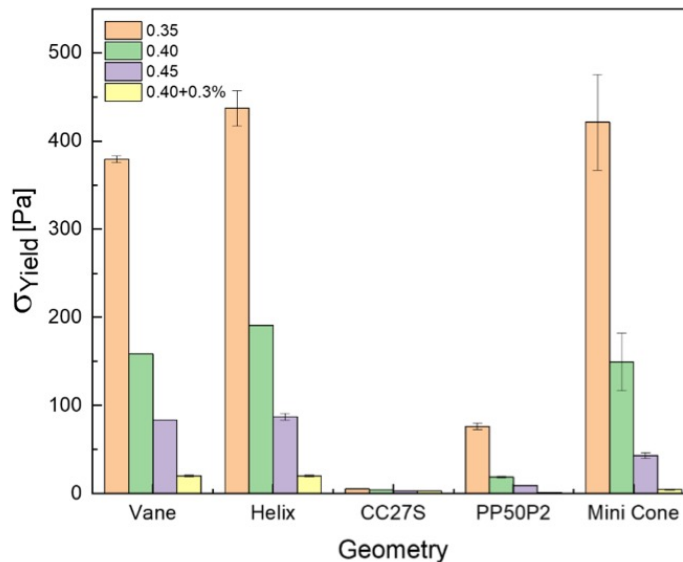
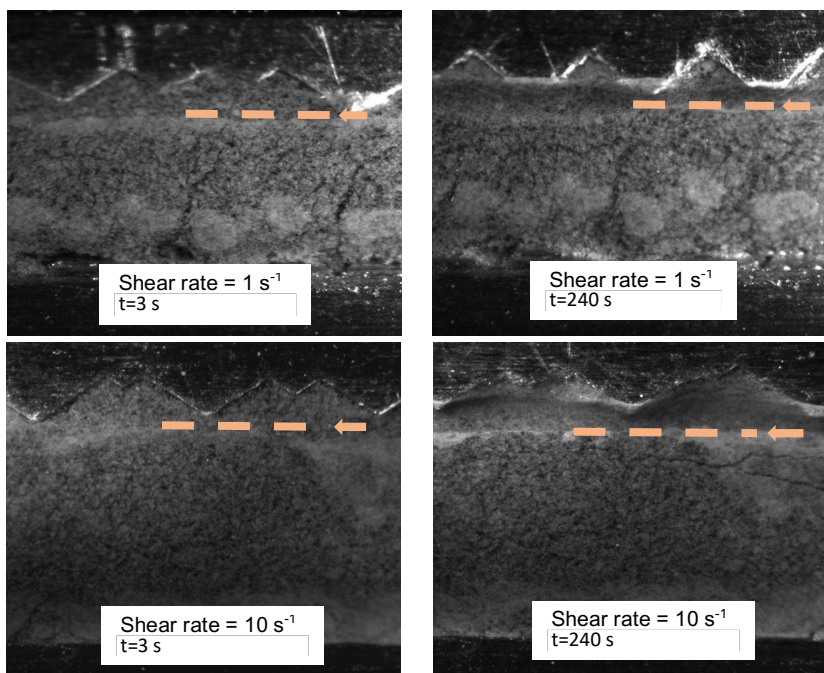


Fig 3.2: Yield stress (σ_{yield}) of cement pastes measured using different geometries, i.e., vane, helical, co-axial cylinders with sand blasted walls (CC27S) and serrated parallel plates of diameter 50 mm (PP50P2), and with mini-cone spread test. Color represents cement concentrations: w/c = 0.35 (orange), w/c = 0.40 (green), w/c = 0.45 (purple), w/c = 0.40 + 0.3% PCE (yellow).

Results show that yield stresses measured using vane and helical geometries match with the ones measured using mini-cone spread tests. On the other hand, the values of the yield stress measured using co-axial cylinders geometry and parallel plates are considerably low. The small size of the error bar in rheological measurements depicts the high reproducibility of the data.

Observing the flow pattern during rheological testing was only possible in the plate-plate geometry where the side of the sheared cement paste was imaged. Experiments were performed on the w/c=0.4 paste at different shear rates and images were recorded in the first few seconds and after 240 s of continuous shear application. Images from the movies are shown in Fig 3.3. In most experiments, we observed a transition between the moving part of the sample and the static one. The dotted line (light salmon) is placed to indicate this transition.



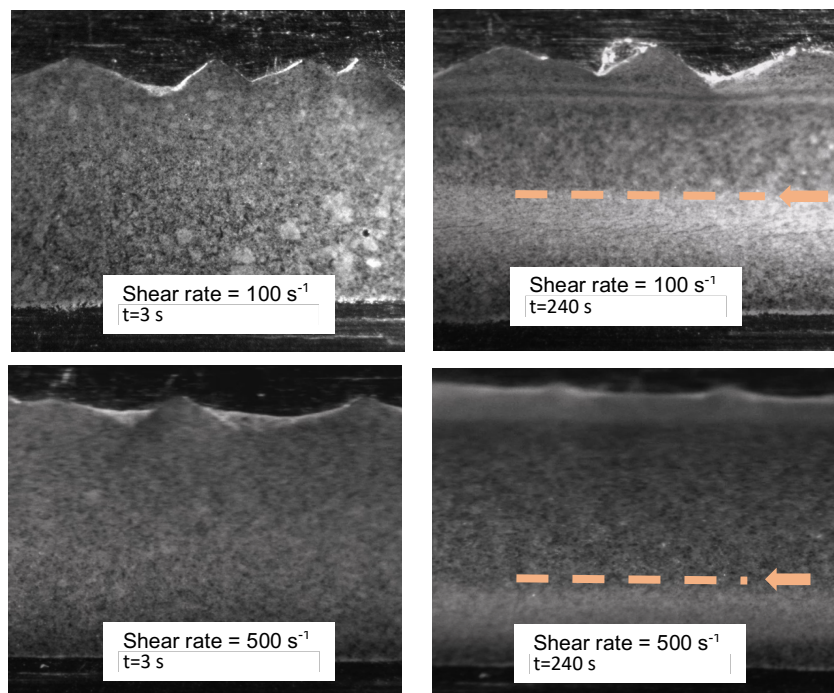


Fig 3.3: Images showing the slurry sample within the gap at the maximum radius. Shear rate and time of photo are indicated on each picture.

Conclusion / Perspectives

This report focuses on the dynamic yield stress measurement of freshly prepared cement pastes using different rheometer geometries and their comparison with the yield stress measured using mini cone spread test. Results show that the yield stress measured with plate-plate and concentric cylinder geometries result in a much lower (unrealistic) yield stress.

Based on local imaging, we conclude that the yield stress of the cement paste determined from the parallel plate geometry is erroneous. This underestimation of stress seems to be linked to the formation of an un-sheared band of paste causing only a small part of the sample to move, likely originating from the formation of a lubrication layer, less concentrated in particles. We predict a similar phenomenon to be happening in case of concentric cylinders geometry but this cannot be imaged using optical tools.

Next, we would like to develop a more reliable data treatment to estimate yield stress from rheology, different from our double derivative method. We plan to also measure the width of the at-rest band, and measure its growth or decrease with time.

References

- Roussel, N., Stéfani, C. and Leroy, R., 2005. From mini-cone test to Abrams cone test: measurement of cement-based materials yield stress using slump tests. *Cement and concrete research*, 35(5), pp.817-822
- Tan, Z., Bernal, S.A. and Provis, J.L., 2017. Reproducible mini-slump test procedure for measuring the yield stress of cementitious pastes. *Materials and Structures*, 50(6), pp.1-12.

Yuan, Q., Lu, X., Khayat, K.H., Feys, D. and Shi, C., 2017. Small amplitude oscillatory shear technique to evaluate structural build-up of cement paste. *Materials and Structures*, 50(2), pp.1-12.

AP 4: Investigation of the influence of the mixing process

Introduction

Ultra-High-Performance-Concretes (UHPC) are limited in their applicability not only due to their high cost (high solid content and additives) but also due to the type of mixers required to prepare them, and the energy cost associated with the mixing: intensive mixers such as EIRICH mixers are powerful but expensive, and offer limited benefit when preparing ordinary concretes.

An alternative for the construction industry is to prepare UHPCs using dry pre-mixes and conventional mixers for the wet mix. In that case, the dry pre-mix needs to be sufficiently homogeneous (particles well dispersed) so that a conventional mixer would be sufficient to get the expected properties, both in fluid and solid states.

In this project, we showed that the main challenge during UHPC dry-mixing is indeed to break down the nano-particle agglomerates of silica fume, and that dry-pre-mixing followed by conventional wet-mixing offers a sustainable alternative for making UHPCs.

Brief summary of results presented in earlier reports

In earlier reports the methods and materials were presented. It was shown, that a longer dry mixing duration has a positive influence on wet mixing time (it becomes shorter), on fresh concrete properties (the concrete has better workability) and mechanical properties of hardened concrete (it gets stronger).

It was shown that silica fume is heavily agglomerated and that breaking these agglomerates requires a large amount of energy. This deagglomeration is crucial for the properties of the concrete, as it releases of water trapped in voids within the agglomerates and increases the packing density). The presence of sand during dry mixing supports deagglomeration due to a "milling effect".

In the following part the influence of dry mixing time on particle size distribution on the UHPC mixes by using laser diffraction is reported.

Measuring particle size with laser diffraction

Laser diffraction is a common method to measure the particle size distribution (PSD) of powders. In this work, Mastersizer 3000 from Malvern Instruments was used. The measurement range of this device is from 10 nm up to 3,5 mm. It is necessary to know the two optical parameters refractive index (RI) and absorption index (AI) of the material composing the powder as well as the RI of the dispersant to perform a correct measurement.

In this work, it was not only necessary to measure single materials, but also a blend (mix) of different materials. These were silica fume (SF), cement (C), quartz powder (QP) and fine quartz sand (QS), all with different optical parameters.

The recommended approach to find the right optical parameters to measure the PSD of a blend is by taking the values of the finest powder. Indeed, using laser diffraction, the finest particles usually dominate the result because their number is much larger than the other particles, even when their volume fraction is small.

Therefore, in all our measurements of whole mixes, the optical parameters of SF were used (RI=1,464 and AI=0,005; provided by the manufacturer of SF).

Another very important parameter is obscuration. It represents the concentration of the sample (the powder) in the dispersant. If obscuration is too low, the amount of sample may not be representative. If it is too high, multiple scattering may occur. Multiple scattering occurs when the laser hits (scatters off) more than one particle and results in a larger scattering angle being detected and analyzed by a detector. Because small particles scatter at wider angles than large particles, the effect of multiple scattering is incorrectly analyzed as a larger content of small particles than the real count (Technical Note, HORIBA Instrument). Therefore, when multiple scattering occurs, the PSD measurement is incorrect.

During this period, we found that the mixes used in this work are very sensitive to obscuration. In this particular case, an obscuration around 6-9% lead to stable and correct measurements, i.e. significantly lower than the 10-15% recommended. The PSD of the mix clearly shows three modes, called Mode SF, Mode C+QP and Mode QS. A mode represents the percentage of particle volume within this mode. All three modes together are 100% of the volume.

Figure 4.1 shows the influence of multiple scattering especially on Mode SF, which is the mode of highest interest in this work.

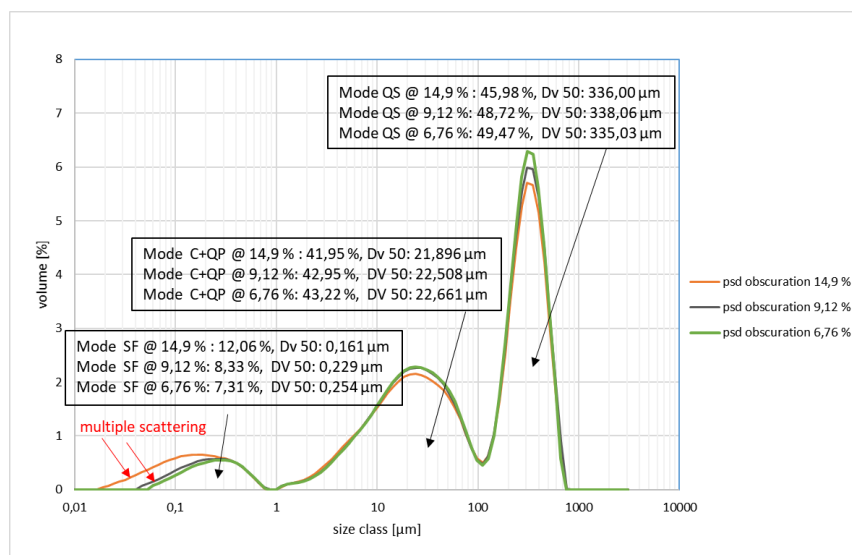


Figure 4.1: Influence of multiple scattering due to high obscuration on PSD and Modes

After the protocol for PSD measurements was defined, 35 measurements of the same mix were performed to validate the reproducibility of these measurements. This mix was 15 min dry-mixed with the EIRICH intensive mixer. The errors for the three modes, Dv 50 for each mode and packing density (PD) of the mix is shown in figure 4.2. Packing density was calculated using the *Schwanda* model.

The error covers both material sampling and the measurement method itself. The errors for each mode are small, giving confidence in the good reproducibility of the method when measurement parameters are kept constant.

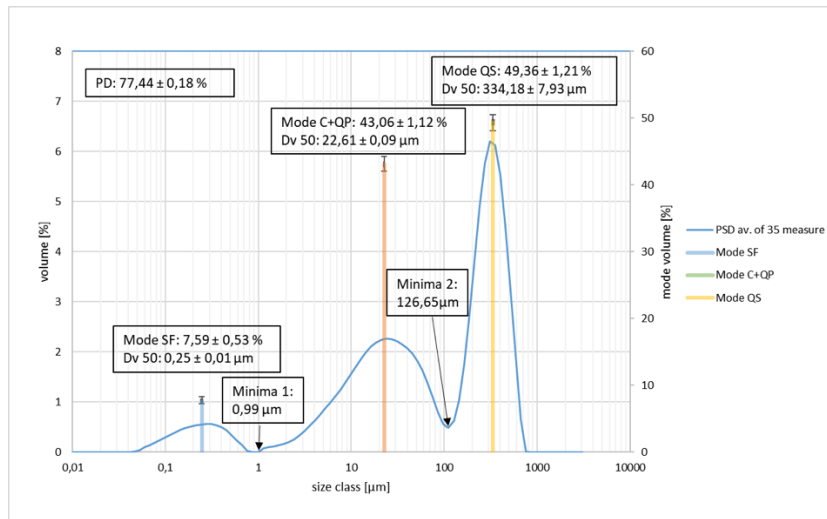


Figure 4.2: Reproducibility and errors of PSD measurement of mixes on PD, modes and Dv 50 of modes

Results

UHPC premixes with a dry mix duration between 90 s and 60 min were prepared, one time with the mortar mixer and one time with the EIRICH intensive mixer. The PSD was measured and the PD calculated.

The main interest was in observing the evolution of the Mode SF. Increasing volume of SF in the PSD shows the deagglomeration of SF, which is the main goal of the dry mixing process with the intensive mixer and the main focus of this project. Figure 4.3 illustrates the influence of dry mix duration on Mode SF and compares both mixers.

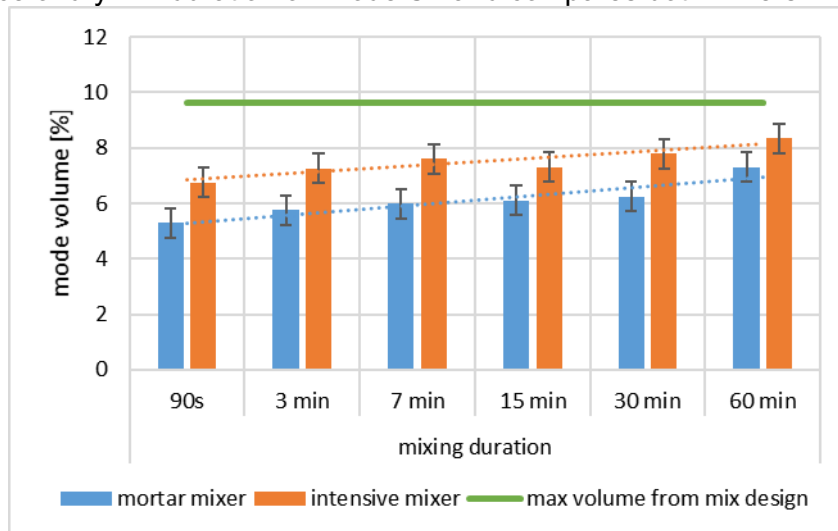


Figure 4.3: Influence of dry mixing duration on the Mode SF (Volume of silica fume in the mix)

Results show a clear trend: the SF mode (associated to de-aggregated silica fume volume fraction) increases with mixing time, with both mixers. They also highlight the difference of power between the mortar mixer and the intensive mixer: the intensive mixer produces the same amount of deagglomerated silica fume in 90 s as the mortar mixer

within one hour. However, even using the EIRICH mixer for 60 min, the theoretical silica fume volume (as per the recipe) could not be reached.

Results Figure 4.4 illustrates the influence of dry mix duration on packing density. The packing density increases with dry mixing time, as a result of a more efficient deagglomeration of silica fume with increasing mixing time. However, the theoretical PD of this mix composition could not be reached. Indeed, the theoretical packing density was calculated with the assumption of fully deagglomerated silica fume.

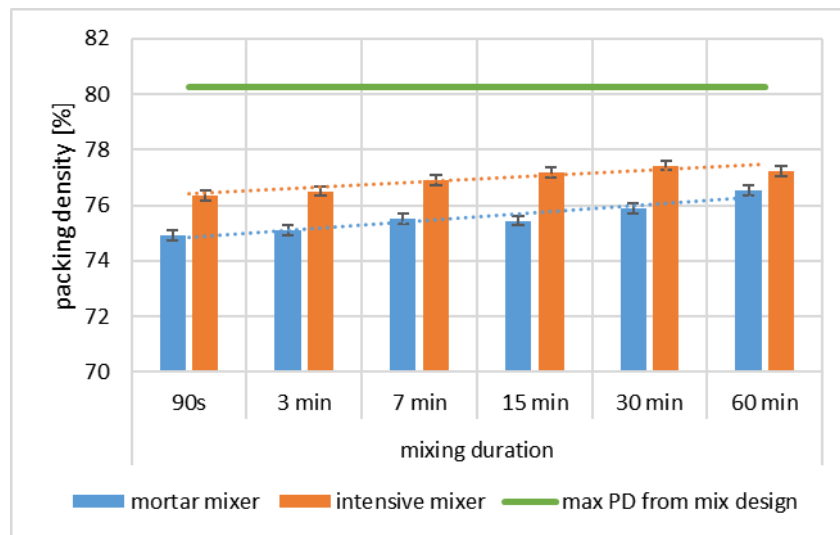


Figure 4.4: Influence of dry mixing duration on the packing density due to proceeding deagglomeration of silica fume

Conclusion

Particle size distribution measurements were performed using a Mastersizer 3000 from Malvern Instruments. A proper protocol was identified, and the importance of the obscuration parameter was highlighted. We showed that maintaining this parameter around 6-9% prevented multiple scattering to occur and gave quantitative results for the smaller particles (in the range 10 nm – 1 mm).

Using the right setup for the instrument, we analyzed the dry mixes produced with a mortar mixer and with the high intensity EIRICH mixer. Results show that increasing dry mixing time increases the volume fraction of deagglomerated silica fume, and in turn the packing density, with both mixers, and that the EIRICH mixer was a lot more efficient at deagglomerating silica fume. It was not possible, however, to fully deagglomerate silica fume by dry mixing within a practical relevant mixing duration.

These results confirm that the high intensity mixer is critical for a quick de-agglomeration of the very fine particle (in the range 10-500 nm). They also show the importance of dry mixing time for the preparation of pre-mixes and can explain the positive influence of longer dry mixing times on the properties of UHPC made from pre-mixes.

Literature

HORIBA Instruments, Effect of concentration on laser diffraction measurements, Technical note LA Series TN162

AP 5: Influence of cement particle size distribution and nature (presence of sustainable binders) on concrete rheology, foamability, and setting properties

In this case study, yield stress and elastic modulus measurements are performed on several formulations of an alkali-activated binder (AAB) and on an ordinary Portland cement (OPC). As a natural continuum from last year study, we decided to explore several AAB formulations studying the compatibility with PCE (poly-carboxyl ether), a classic superplasticizer for OPC. It is well known that OPC has energy-intensive manufacture, which makes it essential to look for low-energy alternatives as alkali-activated materials. The AAB formulation used here (Buchwald et al. 2015) is slag-based, and it uses two solid activators to further reduce the environmental impact. One of the main limitations of AAB is the limited workability of the fresh paste, further limited by the inefficacy of superplasticizers which are ordinarily used for cement-based slurries (Palacios et al. 2009). Indeed, numerous studies have shown no effect of superplasticizers on alkali-activated slag-based materials (Tong et al 2020). We hypothesize that the reason behind these contrasted behaviors is their chemical compositions, and, in particular, the calcium concentration in the pore solution of the two cementitious materials. The amount of calcium in OPC after mixing is indeed around 20 mM (Taylor 1997, Nachbaur et al. 1998), while in AAB instead, it is around 1 mM (Bernal et al., 2015). For this reason, we first tried to match the chemical composition of OPC in AAB by adding calcium ions, and subsequently, quantify the efficacy of PCE in AABs with and without added calcium.

Materials and Methods

The formulation of the AAB used in this study is (by weight) 91.5 % of slag (Ecocem, France), 5 % of NaCO_3 , and 3.5 % of Ca(OH)_2 (Purdon, Patent 1935). As OPC, we used Der Blaue CEM I 52.5 R (Lafarge, Austria).

In order to increase the calcium content in AAB without affecting the pH, we added 5, 10, and 20 mM of CaCl_2 . For example, for 20 mM of CaCl_2 , 2.2 g of calcium chloride are dissolved in 1 L of distilled water, and this solution is then used to obtain cement pastes. In total, we studied 5 compositions: AAB, AAB_5 (i.e. 5 mM CaCl_2), AAB_10, AAB_20 and CEM (i.e. Der Blaue), tested with and without 0.25 wt. % of PCE.

For methods, please refer to last year report.

Results & Discussion

In Fig. 5.1, the values of the elastic modulus G'_{lin} for the 5 compositions with and without PCE are shown.

Adding 0.25 wt. % of PCE on cement shows a very strong effect, as expected. Looking at the alkali-activated series, for both AAB and AAB_5, no visible effect occurs upon addition of PCE. Starting from 10 mM of CaCl_2 , the PCE shows an effect that becomes important on AAB_20. Indeed, the value of the linear elastic modulus reduces by more than half in presence of 20 mM of CaCl_2 and 0.25 wt. % of PCE. This effect on AAB was

never observed before (Tong et al 2020). The value of G'_{lin} is linked to the cohesivity of the paste (Shih et al. 1990). By changing the composition of the pore solution upon addition of calcium ions, the interactions between AAB particles are different and more similar to the ones of OPC. The most evident confirmation of this analysis is the effectiveness of PCE on AAB_20.

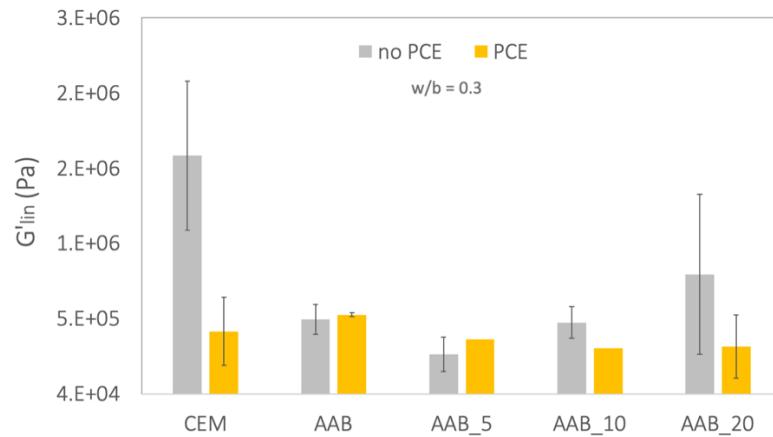


Fig.5.1: Linear elastic modulus G'_{lin} for the 5 different samples with and without 0.25 wt. % of PCE.

The PCE effect on the dynamic yield stress of OPC, AAB, and AAB_20 obtained by mini-cone spread is shown respectively in Fig. 5.2, 5.3, and 5.4. The slurry properties were assessed for up to one hour.

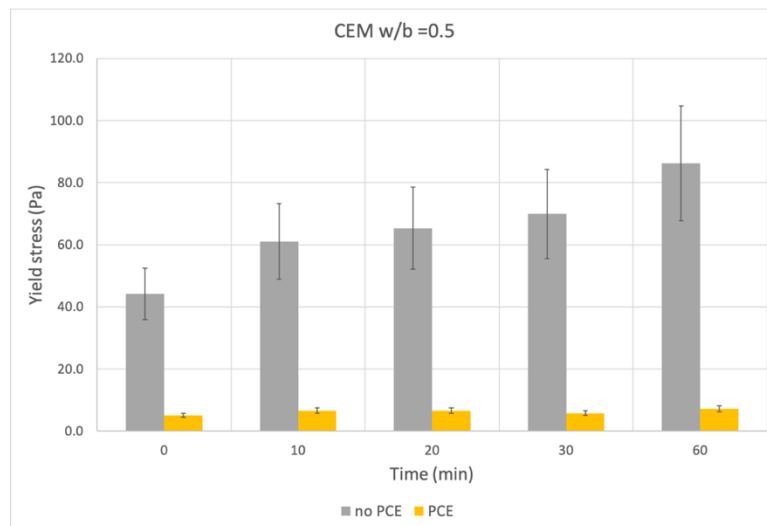


Fig. 5.2: Dynamic yield stress as a function of time for OPC slurries at w/b=0.5 with and without 0.25 wt. % of PCE.

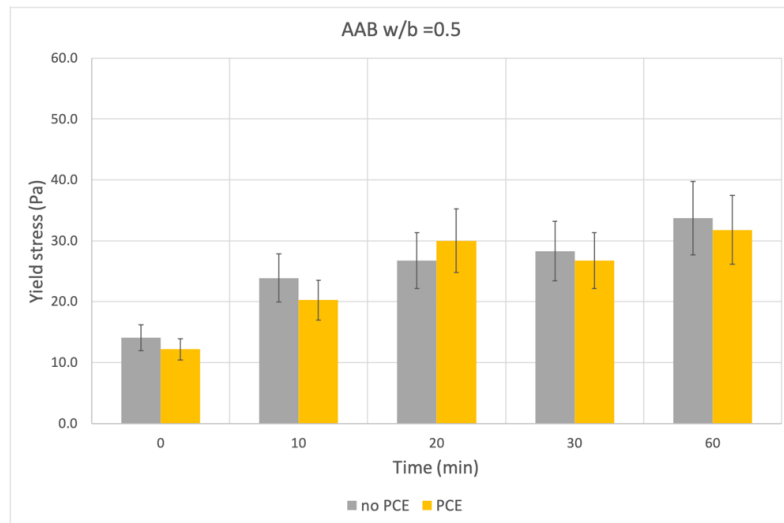


Fig. 5.3: Dynamic yield stress as a function of time for AAB slurries at $w/b=0.5$ with and without 0.25 wt. % of PCE.

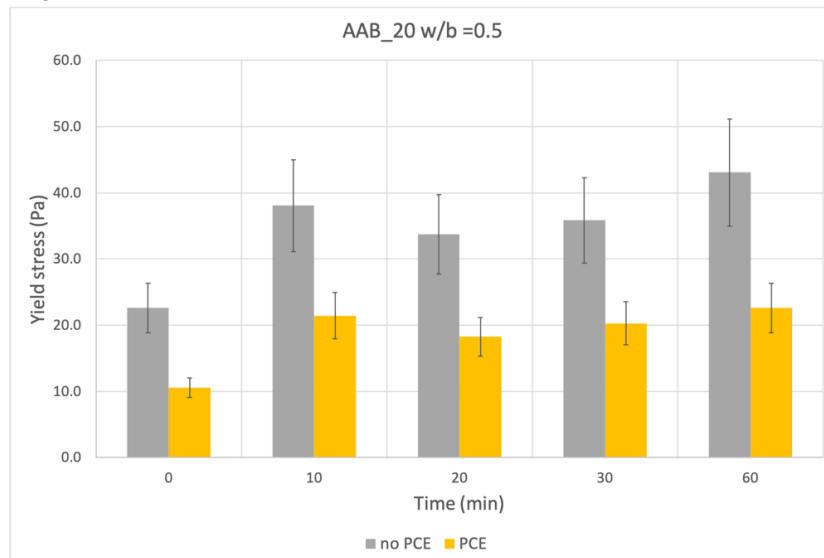


Fig. 5.4: Dynamic yield stress as a function of time for AAB_20 slurries at $w/b=0.5$ with and without 0.25 wt. % of PCE.

Results show that PCE is highly effective in reducing the dynamic yield stress of cement (as expected), and has a lasting effect on the time scale explored here (one hour). On the other hand, the superplasticizer shows almost no effect on AAB yield stress, aligned with G'_{in} measurements, but strikingly reduces by a factor 2 the yield stress of AAS_20 at all times. In other words, this fluidifying effect of PCE is kept for at least one hour on AAS where the calcium concentration was artificially enhanced to reach a similar value to OPC. Also, the trend of the three systems matches with the result obtained at rest (linear elastic modulus).

Conclusion & Perspective

In this study, we have compared the properties at rest (linear elastic modulus) and under flow (yield stress) of OPC and a classic AAB formulation. These two systems react

differently to PCE, a well-known result from practitioners and documented in literature. We observe a clear change in the behavior of AAB enriched with calcium ions at a similar level to the ones in OPC (ca. 20 mM). Indeed, a small amount of PCE added to AAB_20 decreases both the cohesion (G'_{lin}) and the workability (yield stress) of the slurry. This result is indicative of a modification of the surface properties (charge density and surface potential), which affects the particle interactions, the floc self-assembly, and consequently the behavior upon the addition of superplasticizer.

Next, we plan to perform mechanical characterization of OPC and AAB after setting, and extend this study to other slag-based formulations.

References

Bernal, S.A., Provis, J.L., Myers, R.J., San Nicolas, R. and van Deventer, J.S., 2015. Role of carbonates in the chemical evolution of sodium carbonate-activated slag binders. *Materials and Structures*, 48(3), pp.517-529.

Buchwald, A., Vanooteghem, M., Gruyaert, E., Hilbig, H. and De Belie, N., 2015. Purdocement: application of alkali-activated slag cement in Belgium in the 1950s. *Materials and Structures*, 48(1), pp.501-511.

Dhasindrakrishna, K., Pasupathy, K., Ramakrishnan, S. and Sanjayan, J., 2020. Effect of yield stress development on the foam-stability of aerated geopolymer concrete. *Cement and Concrete Research*, 138, p.106233.

Nachbaur, L., Nkinamubanzi, P.C., Nonat, A. and Mutin, J.C., 1998. Electrokinetic properties which control the coagulation of silicate cement suspensions during early age hydration. *Journal of Colloid and Interface Science*, 202(2), pp.261-268.

Palacios, M., Houst, Y.F., Bowen, P. and Puertas, F., 2009. Adsorption of superplasticizer admixtures on alkali-activated slag pastes. *Cement and Concrete Research*, 39(8), pp.670-677.

Purdon A. O., Improvements in processes of manufacturing cement, mortars and concretes, British Patent GB427 227 (1935).

Shih, W.H., Shih, W.Y., Kim, S.I., Liu, J. and Aksay, I.A., 1990. Scaling behavior of the elastic properties of colloidal gels. *Physical review A*, 42(8), p.4772.

Taylor, H.F., 1997. *Cement chemistry* (Vol. 2, p. 459). London: Thomas Telford.

Tong, S., Yuqi, Z. and Qiang, W., 2020. Recent advances in chemical admixtures for improving the workability of alkali-activated slag-based material systems. *Construction and Building Materials*, p.121647.

Gypsum reactivity – Preliminary results

Related to WP8, we use oscillatory rheology to assess early reactivity of gypsum mixed with hydrated cement powder. HB and HG are respectively hydrated Der Blaue cement powder and hydrated gypsum powder (manufacturing detailed in WP8). Early results (Fig 5.5) show that upon adding HG to HB, the paste gets stiffer very quickly (initial G'). Then, the reactivity of the HB+HG mixture seems to be similar to the reactivity of the HB alone.

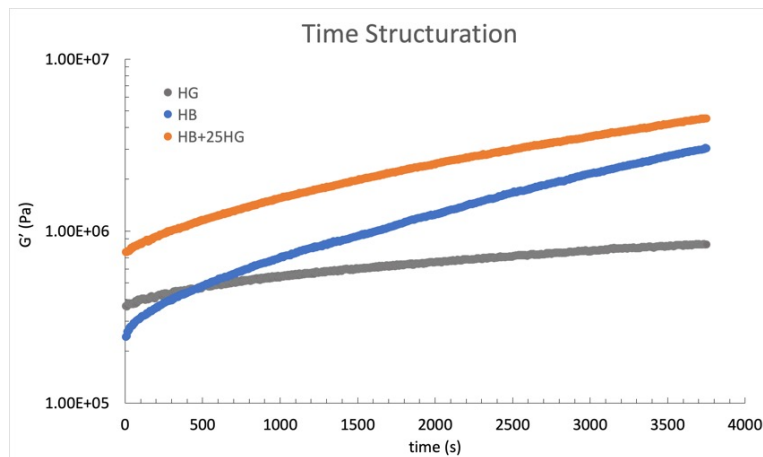


Fig. 5.5: Time structuration of HB paste at $W/C= 0.5$ (blue line), HG paste at $W/C= 0.67$ (grey line), and HB+25HG $w/HB=0.5$ (orange line)

Influence of aluminate phase on early reactivity using XRD and isothermal calorimetry (collaboration with Dr Bellotto, Univ Padova, Italy) – Preliminary results

Below are preliminary results to confirm the influence of the aluminate phase on early reactivity of cement.

Der Blaue (CEM I 52.5 R), Der Contragress (C_3A -free), and pure tricalcium silicate (C_3S) pastes were prepared with a ratio $w/s=0.4$. Heat flux was measured during 24+ hours. Results (Fig. 5.6) show that the main hydration peak of the CEM I occurs about 2 hours before the peak of Der Contragress and of C_3S , that occur at the same time.

The reactivity of pure ettringite paste with a $w/s=0.6$ was also assessed by preparing a blend of calcium aluminate + $Ca(OH)_2$ + gypsum in stoichiometric condition (Fig. 5.7). Only one peak can be seen at about 20 min after mixing.

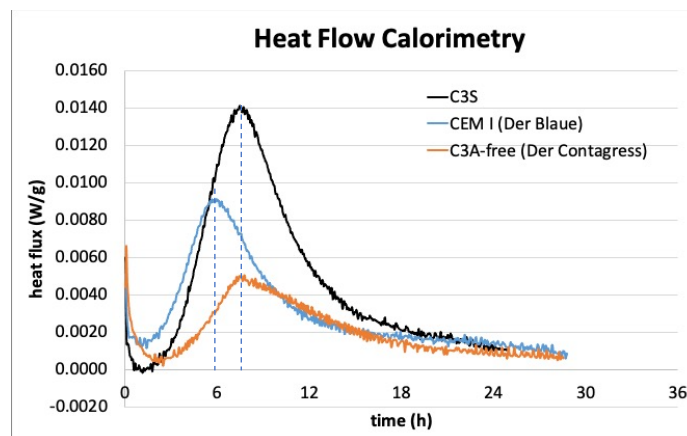


Fig. 5.6 – Heat flow calorimetry on Der Blaue, Der Contragress and a pure tricalcium silicate C_3S paste.

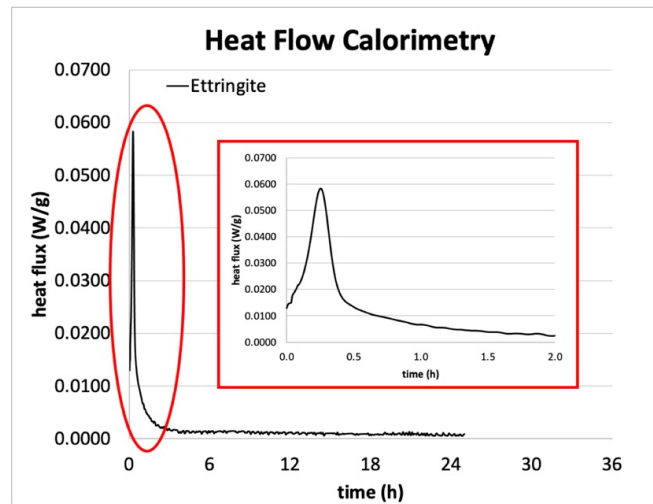


Fig. 5.7 – Heat flow calorimetry on a stoichiometric mixture of calcium aluminate + $\text{Ca}(\text{OH})_2$ + gypsum to produce ettringite.

XRD measurements of these materials were also conducted for 24 hours and a model was used to calculate a theoretical heat flux (Univ. Padova). Calculations from the XRD data matches rather well with the calorimetry data (Fig. 5.8).

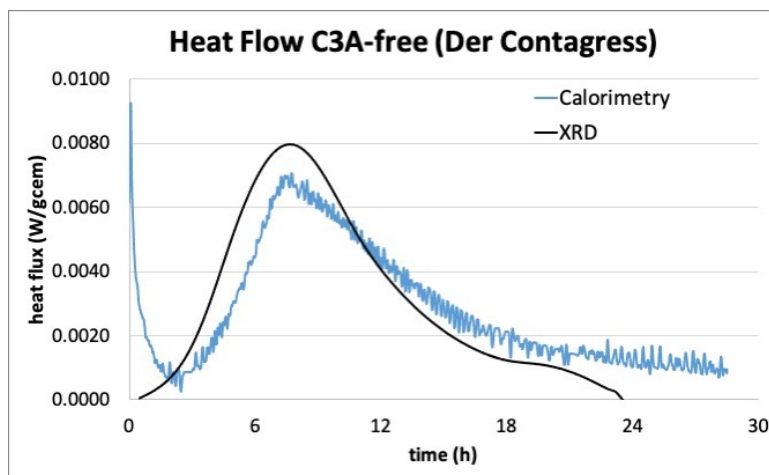


Fig. 5.8 – Experimental heat flow calorimetry results compared to prediction from XRD measurement on Der Contagress.

AP6: Interfaces between old material and new concrete

Introduction

Last year results showed a clear effect of temperature on concrete-epoxy-concrete bond strength (using pull-off tests, wedge splitting tests and bi-surface shear tests). This year, we investigated the behavior of epoxy and cement alone at these temperatures, as well as the microstructure of the interface, successfully explaining the macroscopic mechanical results.

Materials and Methods

The viscosity of epoxy samples was measured at studied temperatures, namely 5, 15, 25, 35, 45, 55 °C using a rheometer (*Anton-Paar MCR 302*) with a 25 mm plate-plate geometry. Two types of samples were prepared, one with epoxy only and the other containing quartz sand, as used for the production of the concrete samples.

The evolution of shore D hardness of the epoxy was measured as a function of time at all studied temperatures for 7 days. After 7 days, the samples were taken out of the climate chambers and kept in the lab ambient condition for 21 more days (like composites were) and the shore D hardness was measured again at the end of this stage. Using the hardness measurement versus time, the epoxy initial and final curing times were defined. The initial curing time, sometimes called open time, is the time period during which the epoxy remains liquid (shore D hardness of zero). The open time is an important indicator of the time that epoxy remains workable enough to be spread on surfaces. The final curing time was defined as the time it takes for epoxy to reach 90 % of its 7-day shore D hardness value.

Parallel to epoxy characterization, the initial and final setting times of the cement paste were determined using *Controls automatic Vicamatic-2* (model 63-L2700/PR) according to the standard EN 196-3. The needle diameter was 1.13 mm and penetrations were automatically performed at intervals of 10 minutes. The test was adapted to measure the setting times at all studied temperatures.

The microstructures of epoxy bonded concretes were characterized using both optical and scanning electron microscopy techniques, after proper sample preparation (cutting and polishing), and image treatment using ImageJ (Fig. 6.1).

Back Scattered Electron (BSE) imaging was used to observe the microstructures of cement based materials with the advantage of distinguishing the constituting phases based on their atomic number (not shown here).

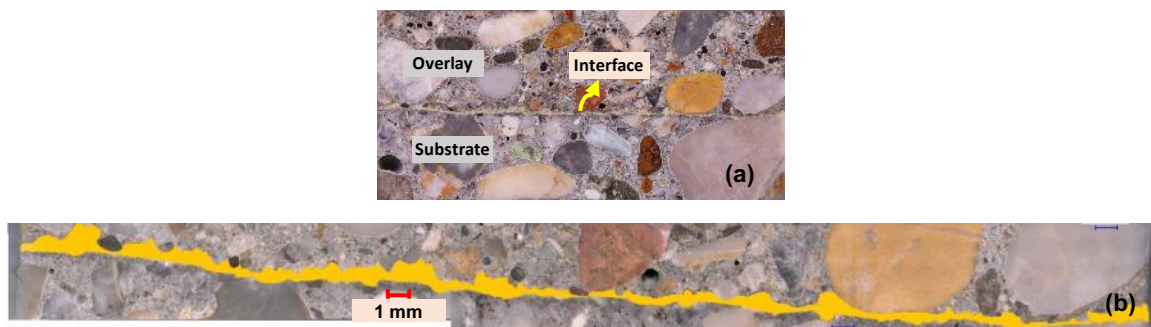


Fig. 6.1 Epoxy layer characterization, (a) image of polished sample, (b) highlight of epoxy layer from optical micrograph (image segmentation)

Results and discussion

Results show that the viscosities of both epoxy and the epoxy-quartz sand samples exhibit a drop by about one order of magnitude when the temperature increases from 5 to 55 °C (Fig. 6.2 left). This drop correlates with the decrease in epoxy mean thickness in the sample cast and set at the same temperatures (Fig. 6.2 right).

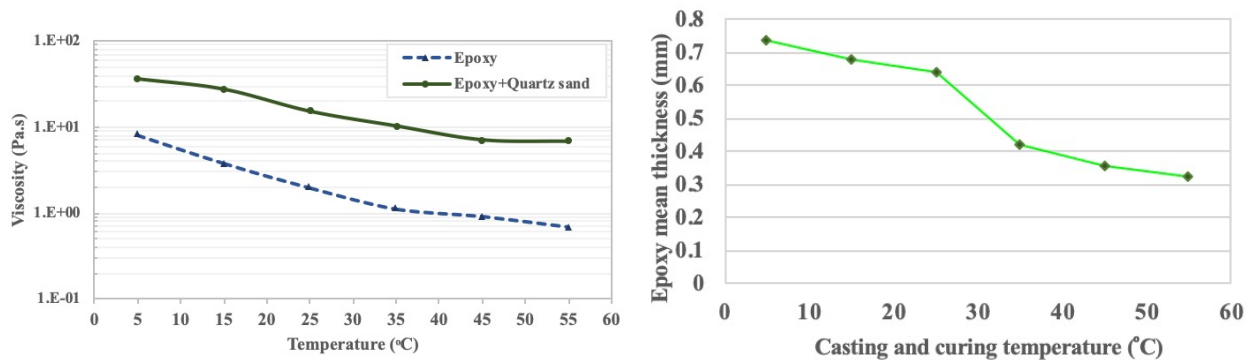


Fig. 6.2 Left: Viscosity of epoxy and epoxy-quartz sand measured at 50 s^{-1} function of temperature Right: Epoxy mean thickness after final curing function of casting and curing temperature

Fig. 6.3 shows the initial and final setting times of cement paste and of epoxy (with the same recipes than those used in composites). As expected, the temperature influences both the epoxy and cement paste setting times. The graph clearly shows that the setting time windows of epoxy and cement barely overlap at 35, 45 and 55 °C, reducing the likelihood of proper physical and chemical interactions between the epoxy and the overlay concrete (specifically C-S-H and Portlandite) (Djouani et al, 2011). Indeed, fractures are, in all cases, adhesive at these temperatures.

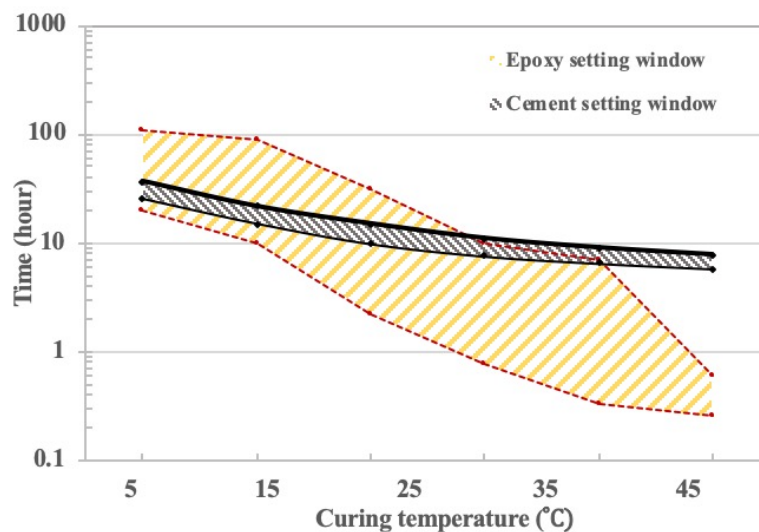


Fig. 6.3 Epoxy and cement paste setting times function of temperature

Conclusion

In this study, three main factors contributing to the decreased interfacial bond strength with increasing casting and curing temperature were identified.

The setting of epoxy at high temperatures (35, 45 and 55 °C) was measured to be considerably faster than the setting of cement at these temperatures, preventing the development of interactions between epoxy and cement in the overlay. Post-mortem 35, 45 and 55 °C sample observations confirm this hypothesis, showing that fractures occur

along the epoxy/overlay interface in all cases. The significant differential setting time between the epoxy and fresh overlay is considered as a key factor negatively impacting the interfacial bond strength of epoxy bonded concretes.

The increase in temperature also drives a decrease in bonding agent average thickness in the composite, following a reduction of viscosity with temperature (loss into microcracks and pores of the concrete substrate), weakening the interfacial adhesion and decreasing bond strength.

Finally, the surface hardness measurement of the epoxy revealed that the 28-day shore D hardness of the high temperature cured epoxy samples is lower (up to 18 %) than the ones cured at low temperatures (not shown here). The inferior mechanical properties of epoxy at high curing temperatures may be another reason behind the lower interfacial bond strength of epoxy-bonded concretes.

To mitigate the detrimental effects of temperature, job times should be adjusted to avoid hot hours. Also, accelerating the cement hydration or retarding the epoxy setting would provide a more gradual hardening of the epoxy and hence a better overlapping with cement setting.

References

- EN 196-3, Methods of testing cement–Part 3: Determination of setting times and soundness, (2016)
- F. Djouani, C. Connan, M. Delamar, M.M. Chehimi, K. Benzarti, Cement paste-epoxy adhesive interactions, *Constr. Build. Mater.* 25 (2011) 411–423.

AP7: Device for the measurement of infiltration

Introduction

Infra lightweight concretes have gained popularity in the past decade, with the work of Schlaich (Elshahawi et al, 2020). These concretes are not only lightweight, but they have low thermal conductivity and reasonable compressive strength (10 to 20 MPa), enabling the construction of monolithic buildings where the material composing the walls is both structurally load carrying and at the same time thermally insulating. Such materials are typically made by mixing lightweight aggregates (expanded clay, expanded glass and foamed glass) with a cementitious binder.

The main concern with such materials in their fresh state is the water absorption capacity of porous aggregates that makes the concrete unworkable. Two options are typically used: either the aggregates are pre-soaked, or extra water is added to the concrete mixture to account for this absorption. This extra water may, in turn, lower the concrete strength or introduce defects resulting from large bleeding and slurry instability.

Here, we investigate a novel method to manufacture such concretes. We infiltrate a pack of porous aggregates with a slurry from bottom up. In other words, in the real field application, the porous aggregates would be placed within the formwork and the slurry pumped from bottom up. This method has the potential to obtain a concrete with a higher content of aggregates by maximizing their packing (the thermal conductivity, the density and the cost will decrease further), use a lower content of cement (the concrete is more sustainable), while increasing mechanical properties by minimizing the water-to cement ratio. The challenge here is the risk of filtration issues: porous aggregates tend to suck the water out the slurry, de-watering it and leading to a denser and thicker paste,

eventually leading to the blockage of the flow, an issue common to grouts (Draganović & Stille, 2011).

In this study, we infiltrate a pack of aggregates placed in a pipe with a cement slurry. In the experimental campaign, we investigate the following parameters:

- diameter of acrylic tube (the container)
- size and size distribution of expanded clay aggregates
- pre-wetting of expanded clay aggregates
- use of additives in the cement slurry

Materials and Setups

The device built for the measurement of infiltration was made of an acrylic tube, a screw pump (company Mladek), a pressure sensor (Cerabar PMC21) and a funnel to connect the pipe to the plexiglas tube while minimizing flow disturbance entrance effects. The funnel is sealed to the acrylic tube with epoxy glue. Finally, a ball valve is added between the pump and the entry of the pipe.

In preliminary experiments, the porous beads were placed in the pipe and the cement slurry was dropped from the top, penetrating only by gravity. During these experiments, we observed that the slurry flowed preferentially near the walls where packing is less (Fig. 7.1 left). The bottom up setup was built to mitigate this effect, as the fluid diffusing front is stabilized by gravity, parallel but opposite to flow direction, and flat (Fig 7.1 right).

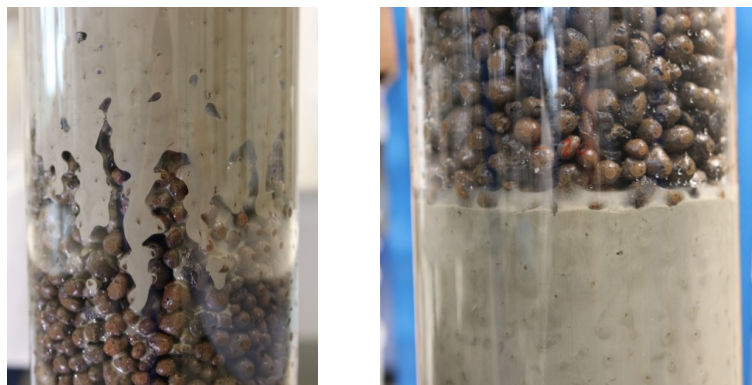


Fig. 7.1 – Slurry diffusing front in (left) experiment where slurry is dropped above pack and penetrates by gravity (right) bottom up pumping

The wall steric hindrance was highlighted using hydrated concrete samples. Sections of clay beads infiltrated with cement slurry were cut through a pipe section after hardening was sufficient (Fig. 7.2). Images were taken and the particle local solid volume fraction was measured as a function of radius using ImageJ software.

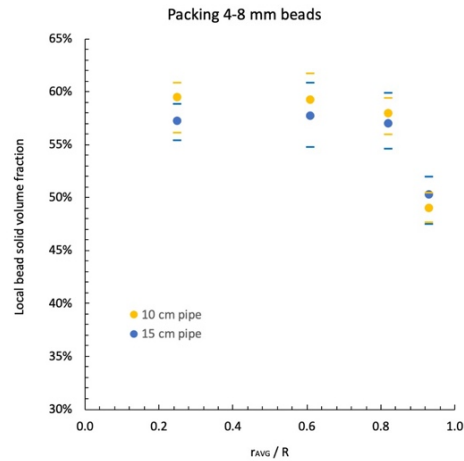
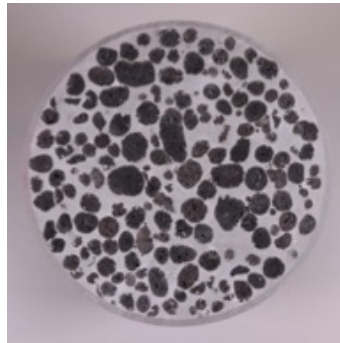


Fig. 7.2 – Left: Probe of hardened lightweight concrete (clay beads infiltrated with cement slurry) for evaluation of wall steric hindrance effect. Right: Measured local solid volume fraction of beads as function of distance from the wall.

Infiltration experiments - Results

Results from table 7.1 show that it is especially difficult to infiltrate a pack of porous clay beads with a cement slurry when the beads are not pre-wetted (saturated with water). None of the slurries could infiltrate the pack if the aggregates were not pre-saturated in water, except that one that contains the oilfield additive (B5). This last result is remarkable.

Tab. 7.1 – Results of infiltration experiments.

-	Tube	Leca		pre-wet	w/c	PCE	spread	funnel	infiltration
-	ø[cm]	ø[mm]	h [cm]	yes/no	-	[%]	[cm]	time [s]	yes/no
B1	15	8-16	85	yes	0,4	0,35	29,5	1,8	yes
B2	15	8-16	85	no	0,4	0,45	28	2,3	no
B3	10	4-8	85	yes	0,4	0,35	30,5	1,8	no
B4	10	4-8	15	yes	0,4	0,35	29,5	1,75	yes
B5 ²	15	8-16	85	no	0,4	0,65	38	1,45	yes

²with 0,5 sk/gal of gas migration agent

When the beads are not pre-wetted, a process called *filtration* occurs. Upon flow, the cement slurry loose water to the porous aggregates, making the slurry thicker and thicker, until the slurry is so rich in particles that it cannot flow anymore and gets stuck, blocking further fluid to infiltrate the pack of aggregates. It is important to also note that when the aggregates are pre-saturated, defects can happen when the slurry is dropped from above, as water gets trapped within the concrete sample (Fig. 7.3). In the case of filtration from bottom instead, the extra water accumulates at the top of the slurry front and does not create heterogeneities (and potential defects in the concrete), a potential advantage of the technique.

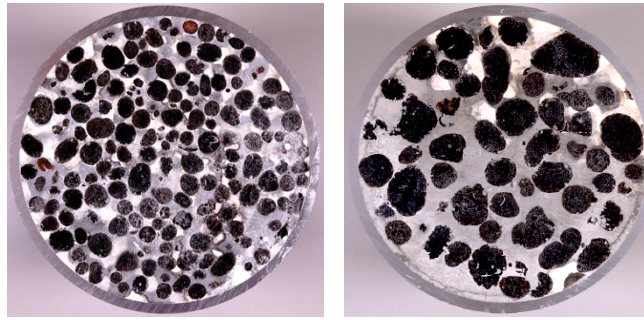


Fig. 7.3 – Hardened expanded clay bead concrete – Defects due to water separation appear white.

Conclusion / perspectives

We proposed here a novel method to produce lightweight structural concretes through an infiltration method, where the lightweight aggregates (LWA) pre-fill the structure and the cement slurry is pumped from the bottom.

We studied expanded clay beads as LWA. We showed that they absorb 10-12 wt. % of water during the first couple of seconds of water exposure. This explains the difficulty of a cement slurry to penetrate such a pack of porous aggregates that have not been previously water saturated.

We indeed measured that when a slurry was pumped through the non-pre-wetted aggregates, a filtration process occurred, leading to a thickening slurry that eventually plugged the interstitial pores and blocked the flow. We also showed that pre-wetting could introduce heterogeneities in composition, potentially decreasing the strength of the hardened concrete.

Importantly, we identified a promising additive that enabled a cement slurry to infiltrate a pack of 85 cm height of non-pre-wetted LWA without any issue, when all other slurries (even as they contained superplasticizers) failed to do so.

Next, several improvements will be pursued. First, while our current bottom up setup allowed us to perform proof of concept experiments, it is limited in terms of pressure resistance (Plexiglas pipe, sealing using silicone, etc). Also, the pressure sensor gave unusable values. Therefore, we will focus next on producing a setup with higher pressure resistance, with pressure measurement, and better flow control. To get closer to application, we plan to manufacture a wall membrane, potentially using commercial formworks.

We also need to focus on maximizing the packing of lightweight aggregates to minimize the concrete density and maximize thermal insulating capability.

Finally, we plan to test the strength of an optimized concrete produced by such a method.

References

Elshahawi, M., Hückler, A. and Schlaich, M., 2021. Infra lightweight concrete: A decade of investigation (a review). *Structural Concrete*, 22, pp.E152-E168.

Draganović, A. and H. Stille (2011). "Filtration and penetrability of cement-based grout: Study performed with a short slot". In: *Tunnelling and underground space technology* 26.4, pp. 548–559.

AP8: Recycled aggregate concretes: Internal sulfate attacks

We investigate the influence on ISA of key-material design variables such as: water to cement ratio W/C, cement type, cement hydration state, curing and ambient condition, gypsum content and fineness. We use several methods to measure the ISA-induced

expansion, such as: prism length variation, Le-Chatelier expansion rings, and oedometer-cell integrated in a compression device. A selection of the more promising results (Le-Chatelier and oedometer) is presented in the next sections.

Materials and Methods

Hydrated cement powder was manufactured in the lab by preparing cement pastes that were left to harden for 28 days, and then crushed and sieved to obtain a final powder with D50 of approximately 16 μm . The procedure is identical for the three cement types:

- Der Blaue CEM I 52.5 R, Lafarge, Austria (**HB**).
- Der Contragress CEM I 52.5 N - SR 0 WT 38 C₃A-free, Lafarge, Austria (**HC**).
- Supracem 45 quick-setting cement, Schretter & Cie., Austria (**HS**).

The three cements can be ranked in term of aluminum content: Supracem 45 > Der Blaue > Der Contragress. We expect a stronger expansion when a higher content of aluminum-based components is present in the cement. To simulate secondary ettringite formation and accelerate internal sulfate attack, a hydrated and milled gypsum **HG** (Knauf, Germany) is added to the hydrated cement pastes and mortars.

Le-Chatelier Ring (ASTM C452) test is used to follow the expansion of hydrating cements. In order to mimic the internal sulfate attack (Stark et al. 2012), 100 parts of the hydrated cement and 50 parts of the hydrated gypsum are mixed (Tab. 8.1).

Tab. 8.1 – Slurries composition for the three hydrated cements for the Le-Chatelier rings.

Samples	Water [g]	Hyd. cem. [g]	HG [g]	W/C
HB	25	50	25	0.5
HC	37.5	50	25	0.75
HS	37.5	50	25	0.75

Once filled, the ring is confined in the axial direction between two plexiglass plates. A weight of 0.5 kg is placed on the top of the upper plate to allow only a lateral expansion. The sample is then stored under water at room temperature. The contact with water allows further reactions. The zero-measurement of the needle tip distance is performed after 24 hours from sample preparation. Further measurements are made after 7 and 14 days. For each hydrated cement type, two samples are tested.

An *oedometer* cell integrated in a one-dimensional compression device (WILLE Geotechnik) is used to measure the swelling pressures of the hydrated cement-gypsum mixtures (100 parts HC and 50 parts HG). The dry samples are compacted with a hydraulic pressure machine, inserted in the oedometer under a pre-loaded force of 30 kPa ($\sim 0.03 \text{ N/mm}^2$). This step ensures a direct frictional connection and contact between the loading sensor and the compression stamp. Water is added from the lower water-valve and the system switches to displacement-controlled measurement (fixed value) while the vertical stress is measured. If the maximum allowable stress is reached, the system is switched to force-controlled mode and the displacement is then measured. For each cement type, two samples are tested and the stress evolution is followed for ca. 360 h (15 days), ensuring a constant water supply (i.e., water bath) at ambient temperature.

Results & Discussion

In Fig. 8.1 the results from the first and second series of *Le-Chatelier* tests are averaged and shown with an error bar.

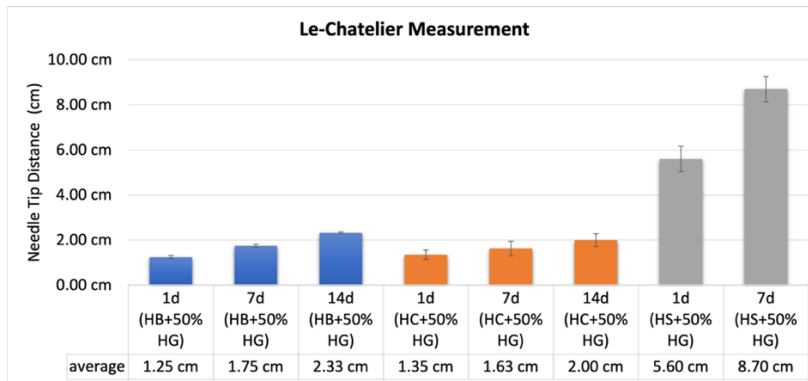


Fig. 8.1: Le-Chatelier measurements for HB, HC and HS cements once mixed with HG after 24h, 7 and 14 days.

A clear trend can be seen from the figure above, confirming our expectations on expansion tendency of the pre-hydrated powders: $HC < HB < HS$. The expansion seems to increase with growing aluminum content in the cement. The expansion of the C_3A -free cement HC may be linked to the presence of residual aluminium compounds (i.e., C_4AF) in the HC that could react with the sulphate ions contained in the HG, forming (secondary) ettringite (Benedix, 2003, Irassar et al., 2000). This effect may need to be further investigated, as it may mean that ISA can represent a hazard also when sulfate-resistant cement is used. HS could only be measured after 24 h and 7 days. This is due to the large lateral and vertical expansion of the sample after 7 days (the upper weight was not sufficient and fell off), making the last measurement no longer representative. The large expansion of HS can be attributed to the high content of residual calcium aluminate (i.e., $C_{11}A_7CaF_2$), responsible also for its rapid setting (Locher, 2000).

The *oedometer* compressive stress measurements resulting from confining the sample are shown in Fig. 8.2 (HB), Fig. 8.3 (HC) and Fig. 8.4 (HS).

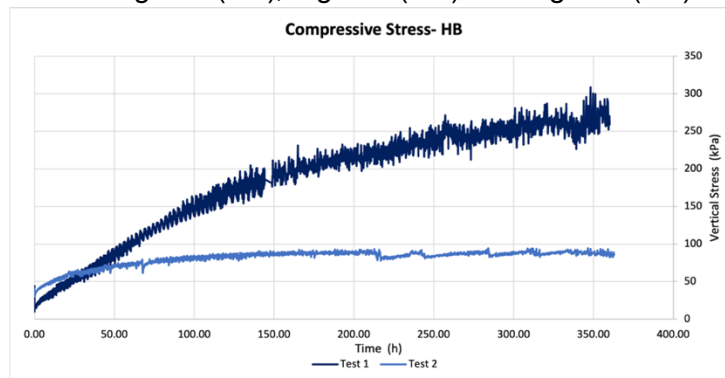


Fig. 8.2: Results of compressive stress measurements – HB.

In the two displacement-controlled measurements of Fig. 8.2, the vertical position is kept constant, and the resulting vertical confining stress is measured. After 15 days, the stress is measured 175 ± 100 kPa. The reason for the large difference between

the two measurements is being further investigated and could be due to variations in sample preparation, such as the degree of compaction.

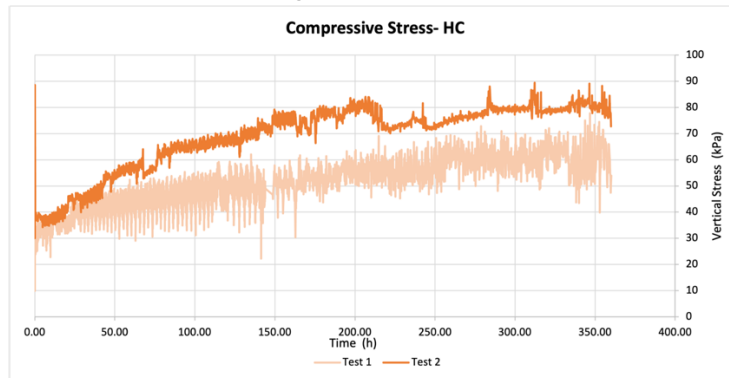


Fig. 8.3: Results of compressive stress measurements – HC.

In Fig. 8.3 for HC, we observe a lower pressure and better reproducibility in comparison with HB. After 15 days, the stress is measured 70 ± 15 kPa.

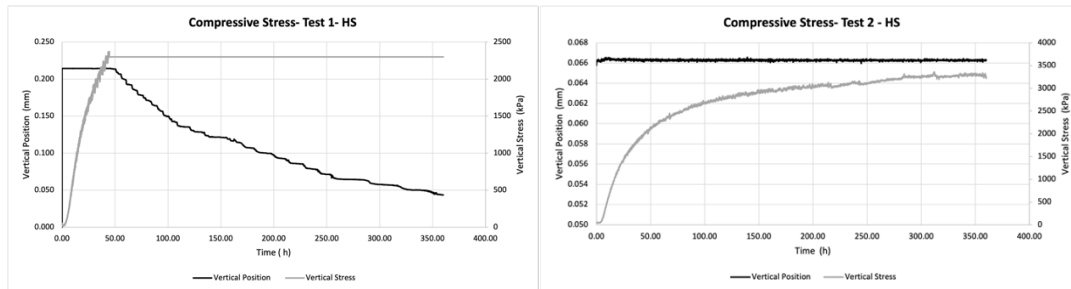


Fig. 8.4: Results of compressive stress measurements – HS.

Fig. 8.4 shows the two tests for HS. During test 1 (left), we observe a rapid increase of the vertical stress (grey line). After 48 h, a stress of more than 2.3 MPa is reached, and the machine is switched to a force-controlled measurement due to reaching its maximum load (2.5 MPa, 5 kN load cell). A constant vertical stress of 2.3 MPa is therefore maintained and the displacement is measured (black line).

Test 2 is performed with a 10 kN cell. The grey curve of the second measurement shows a very similar trend to the first one reaching ca. 2 MPa in the first 48 h. After 15 days, HS reaches a plateau with a stress of over 3.2 MPa, more than ten times higher than HB (≈ 0.25 MPa, Fig. 1.14) and around forty times higher than HC (≈ 0.08 MPa, Fig. 8.3). The measured displacement is mainly due to the swelling pressure resulting from the chemical reaction between water, sulfate, and the aluminates phases in the pre-hydrated cement. The evolution shown by the oedometer measurements for the three cement types are consistent with the results obtained with Le-Chatelier: the confining stress ranks $HC < HB < HS$.

Conclusion & Perspectives

This study was a first attempt to quantify the effect of internal sulfate attacks on various cement types, a complex and controversial problem.

First, we introduced a new measurement to assess the behavior of cement samples in confined conditions adapting an oedometer test protocol. This measurement is complementary from the Le-Chatelier measurements where swelling is unconfined

(in 2D). Indeed, in constructions, the bulk concrete is a under mixed boundary conditions (partially confined) and upon exceeding some swelling pressure, the expansive reaction may result in spalling.

Second, we tested three cements with various content of aluminates phases. Clear trends are obtained for the three hydrated cements in Le-Chatelier and oedometer tests, where volume gain and confining pressure rank as HC (hydrated Contragress) < HB (hydrated Der Blaue) < HS (hydrated Supracem). The measurements on prism length, instead, did not provide consistent results (presented in the ÖBV report).

In order to pursue this topic, we are planning to:

- extend the testing time for prisms,
- secure the confinement in Le-Chatelier to avoid vertical expansion,
- Develop the oedometer setup to control temperature (using thermostatic baths) and test at temperatures above room temperature.
- Substitute Supracem with another cement with a high Aluminium content and a well-known composition,
- repeat Le-Chatelier and oedometer tests with the new aluminium-rich cement and with the same initial slurry consistence.

References

Benedix, R. 2003. *Bauchemie*, Springer.

concrete aggregates. *Construction and Building Materials*, 272, p.121851.

Irassar, E. F., González, M. & Rahhal, V. 2000. Sulfate resistance of type V cements with limestone filler and natural pozzolana. *Cement and Concrete Composites*, 22, 361-368.

Locher, F. W. 2000. *Zement. Grundlagen der Herstellung und Verwendung*.

Stark, J. & Wicht, B. 2012. *Dauerhaftigkeit von beton*.

3. Project team and cooperation

- Are there significant changes in the project team (internal key staff and external partners/third parties)?
- Address changes in the division of labour. Are there any effects on the cost / financing structure and the target?

4. Economic and scientific exploitation

- Describe the exploitation and / or redistribution activities carried out so far. Is exploitation possible?
- List publications, dissertations, theses and any patent applications, which have arisen from the project.
- What further R&D activities are planned?
- How will the prototypes created in the project be further used?

Effect of casting and curing temperature on the interfacial bond strength of epoxy bonded concretes, D. Daneshvar, K. Deix, A. Robisson, *Construction Building Material* (accepted)

Small oscillatory rheology and cementitious particle interactions? T. Liberto, M. Bellotto, A. Robisson (submitted)

FFG-Berichte und Langberichte befinden sich allgemein zugänglich auf der Website der Österreichische Bautechnik Vereinigung

5. Explanations on costs & financing

- Billing is done directly in eCall or, for projects submitted by Sept. 2015, via Excel. In eCall you will automatically be presented with the right variant for you.
- Please refer to the FFG cost guidelines (www.ffg.at/kostenleitfaden) and tender documents.
- Deviations from the cost plan must be described and justified at this point.

6. Project specific special conditions and requirements

- Deal with project-specific special conditions and requirements (according to §6 of the Grant Agreement), if these have been agreed in the Grant Agreement or Contract for Work and Labor.

7. Notifiable events

Are there any special events relating to the funded project which must be notified to the FFG (see also Guidelines - Annex to 5.3., 5.3.5), e.g.

- Changes in the legal and economic possibilities of influencing the Recipient
- Insolvency proceedings
- events that delay the performance of the subsidised service, or render impossible
- Further funding for this project